PROCEEDINGS OF SPIE

SPIEDigitalLibrary.org/conference-proceedings-of-spie

# Development of cryogenic mechanisms for the VLT/ERIS instrument

Adrian M. Glauser, Walter Bachmann, Polychronis Patapis, Mike MacIntosh, Ric Davies, et al.

Adrian M. Glauser, Walter Bachmann, Polychronis Patapis, Mike MacIntosh, Ric Davies, Helmut Feuchtgruber, Stephen March, David Pearson, Sascha P. Quanz, Christian Rau, William D. Taylor, Hans Martin Schmid, Chris Waring, "Development of cryogenic mechanisms for the VLT/ERIS instrument," Proc. SPIE 10702, Ground-based and Airborne Instrumentation for Astronomy VII, 1070230 (6 July 2018); doi: 10.1117/12.2313399

SPIE.

Event: SPIE Astronomical Telescopes + Instrumentation, 2018, Austin, Texas, United States

# Development of Cryogenic Mechanisms for the VLT/ERIS Instrument

Adrian M. Glauser[a], Walter Bachmann[a], Polychronis Patapis[a], Mike MacIntosh[b], Ric Davies[c], Helmut Feuchtgruber[c], Stephen March[a], David Pearson[b], Sascha P. Quanz[a], Christian Rau[c], William D. Taylor[b], Hans Martin Schmid[a], and Chris Waring[b]

[a]Institute for Particle Physics and Astrophysics, ETH Zurich, 8093 Zurich, Switzerland
[b]UK Astronomy Technology Centre, STFC, Blackford Hill, Edinburgh EH9 3HJ, UK
[c]Max-Planck-Institut für extraterrestrische Physik, Giessenbachstrasse 1, 85748 Garching, Germany

## ABSTRACT

We present the design and measured performance of the Aperture Wheel and the Pupil&Filter Wheel mechanisms for the NIX camera of the VLT/ERIS instrument. Both mechanisms were developed for high opto-mechanical precision and stability while operating at 70 K. We summarise the design constraints and considerations. Further, we have developed a dedicated cryo-test facility to allow measuring the position repeatability under nominal operational conditions. We demonstrate that the wheel mechanisms perform as designed and provide the measurement methodology and results of the opto-mechanical tolerances.

**Keywords:** VLT, ERIS, instrumentation, cryo-mechanism, cryogenics

## 1. INTRODUCTION

The Enhanced Resolution Imager and Spectrograph[1] (ERIS) instrument for the Very Large Telescope (VLT) is a 1-5 $\mu$m instrument that will provide diffraction limited imaging and slit and Integral Field spectroscopy (IFS) utilising the Cassegrain focus of UT4 with its new Adaptive Optics Facility. ERIS consists of a wavefront camera,[2] a calibration unit,[3] and the two science subsystems, the IFS SPIFFIER[4] and the NIX-camera.[5]

NIX provides narrow- and broad-band imaging for J-, H-, K-, L-, and M-band, low resolution spectroscopy for L-band, vortex coronagraphy in L- and M-band, and high contrast imaging with Apodised Phase Plates (APP) and Sparse Aperture Masks (SAM). Figure 1 shows the opto-mechanical layout of the NIX-camera. The light passes through the entrance window (not visible in the figure) where shortly after the focal plane is located. The Aperture Wheel (APW) allows placing various field masks and coronagraphic elements in that plane. Thereafter, a camera wheel allows selecting three different camera systems for different plate scales and/or wavelengths. The pupil plane is located just behind the camera wheel where the Pupil&Filter Wheel (PFW) is placed. This mechanism combines a wheel for wavelength filters and a wheel for various pupil masks. To compensate for the different focal lengths of the cameras and to allow pupil imaging capabilities, an image selector mechanism is placed after the PFW, followed by the detector box. A full description of the imager can be found in Pearson (2016).[5] This paper focuses on the development of the APW and PFW, both being developed at ETH Zurich.

ERIS is currently being assembled and is planned for commissioning in 2020. The APW and PFW are going to be integrated in NIX in summer 2018.

## 2. DESIGN CONSTRAINTS AND KEY REQUIREMENTS

### 2.1 Functional Requirements

To support the various observation modes of NIX, dedicated optical elements need to be placed in the focal and the pupil plane, respectively. We provide in Table 1 a list of functions that are supported by the APW and PFW and illustrate the corresponding elements. The APW hosts 8 slots in the entrance focal plane of NIX for

Send correspondence to glauser@phys.ethz.ch

Ground-based and Airborne Instrumentation for Astronomy VII, edited by Christopher J. Evans, Luc Simard, Hideki Takami,
Proc. of SPIE Vol. 10702, 1070230 · © 2018 SPIE · CCC code: 0277-786X/18/$18 · doi: 10.1117/12.2313399

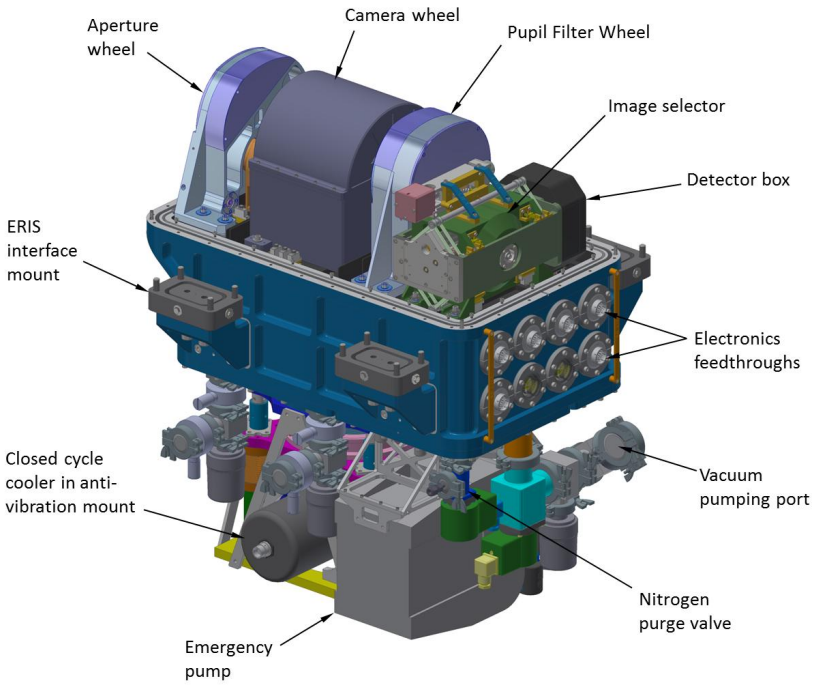


Figure 1. The NIX instrument shown for the opened cryostat

field masks, slits and Vortex-Coronagraphic focal mask. The PFW consists of two wheels, the pupil wheel that is located in the pupil plane of NIX, and the filter wheel, located close to the pupil plane upwards the optical beam. Both wheels have 20 slots which are designed such that the broad and narrow band pass filters could be placed in both wheels interchangeably. However, the pupil wheel is populated mainly with different cold stops,

Table 1. NIX Functions supported by the APW and PFW

| **Function** | **Filter** | **Pupil Mask** | **Aperture Mask** |
|---|---|---|---|
| Short-Wavelength Imaging (JHK-Bands) | J, H, Ks, Pa-$\beta$, [Fe II], H2 cont, H2 1-0S, Br-$\gamma$, IB 2.42, IB 2.48 | Open, Blocking Filter(1) | 26" x 26", 55" x 55" |
| Long-Wavelength Imaging (LM-Bands) | Short L', L', M', Br-$\alpha$, Br-$\alpha$ cont. | Circular Pupil Spider Pupil | 26" x 26" |
| APP Coronagraphy | Short L', L', M', Br-$\alpha$, Br-$\alpha$ cont. | APP incl. Spider | 26" x 26" |
| SAM Imaging | any | SAM-23, SAM-9, SAM-7 | 26" x 26", 55" x 55" |
| L-Band Spectroscopy | L-broad | Grism | 12" x 87 mas slit |
| Focal Plane Coronagraphy | Short L', L', M', Br-$\alpha$, Br-$\alpha$ cont. | Lyot stop + dummy, Lyot stop + ND(2) | Vortex L, Vortex-M |
| Distortion & Image Quality Measurement | any | Open | Distortion grid |
| Blocking | Closed | Closed | Closed |

Note:
(1) The Blocking Filter is used to suppress the fluxes for wavelengths longer then K-band due to the sensitivity of the 5 $\mu$m cut-off HAWAII-2RG detector and the limited suppression level of the short-wavelength filters.
(2) The Combined element Lyot stop + ND is used for flux calibration when the main target is placed off-axis with respect to the Vortex element. As the beam is not collimated, the optical depth between the calibration and nominal science mode needs to be maintained in order to keep the focal length constant. For this reason, a glass dummy with identical optical depth is needed for the nominal science mode.

various pupil masks, a grism, and the APP, while all bandpass filters are located in the filter wheel. One special filter is located in the pupil wheel which is used in combination with the J-, H-, K-Band filters to improve the out-of-band blocking of the red wavelength range, optimising the sensitivity in these observing modes.

Further, the housing between the two wheels of the PFW acts as the Fixed Cold Stop (FCS) for the J-, H-, and K-Band imaging modes (by using a open slot position in the pupil wheel), which require the largest diameter of the cold stop.

### 2.2 Key Requirements

In Table 2 we list some of the key requirements.

Table 2. Key requirements of the APW and PFW

| | **PFW** | **APW** |
|---|---|---|
| Nominal design temperature | 75 K | |
| Operating temperature | 70 - 300 K | |
| Survival temperature | 40 - 353 K | |
| Min. number of slots per wheel | 18 (goal: 20) | 8 |
| Min. rotation speed | 0.75 rpm | |
| Maximum total mass | 6 kg | 4 kg |
| FCS diameter | 13 mm | |

### 2.3 Mechanical Accuracy

The alignment budget of NIX provides the tolerances for the individual components of the instrument. The components will be aligned internally to NIX using mechanical reference points. Relative to these mechanical references, the APW and PFW must provide the following absolute accuracies:

- Lateral displacement in both axis each (radial and tangential): 50 $\mu$m for APW and pupil wheel, 200 $\mu$m for filter wheel.
- Axial displacement: 100 $\mu$m for APW and pupil wheel, 200 $\mu$m for filter wheel.
- Rotational offset - any axis:: 2 mrad

Consequently, the mechanism needs to be build to its own mechanical reference with the mentioned accuracies, incorporating tolerances for manufacturing, flexure, and most importantly, repeatability (between movements) and reproducibility (between different slot location) of the moveable parts. For the 50 $\mu$m displacement, this breaks down to the following internal tolerance budget:

Table 3. Tolerance budget (peak-to-peak) for the displacement in radial or tangential direction for the APW or pupil wheel

| | |
|---|---|
| Absolute position accuracy with respect to local coordinate system | 25 $\mu$m |
| Repeatability of mechanism positioning | 15 $\mu$m |
| Flexure or distortion due to gravity | 10 $\mu$m |
| **Total** | **50 $\mu$m** |

## 3. DESIGN DESCRIPTION

### 3.1 Overview

The basic concept of the APW is shown in Figure 2, the PFW is shown in Figure 3. Key features of the two mechanisms are summarised in Table 4.

The space between the Camera Wheel and the Image Selector of NIX is very limited (see Figure 1). Therefore, the filter and the pupil wheel have been merged in a single mechanism unit sharing the same main structure. Besides of that, the APW and the two wheel mechanisms of the PFW use the same driving architecture: A Phytron VSS 32 stepper motor actuates a worm gear that translates the motion to the wheel using a gear ratio of 1:60. The choice for a worm gear was based on its self-locking behaviour, allowing to power off the stepper

Table 4. Key features of the PFW and APW

| | **PFW** | **APW** |
|---|---|---|
| Number of wheels | 2 | 1 |
| Number of slots | 20/20 | 8 |
| Tested rotation speed | ≤2 rpm | |
| Power dissipation per wheel | ∼1 W/wheel | |
| Total mass | 5.3 kg | 3.5 kg |
| Dimensions (X/Y/Z)(1) [mm] | 85 / 320 / 257.5 | 99 / 320 / 240 |
| Main material | AL 6082 | |
| Stepper motor | Phytron VSS 32.200.1,2 | |
| Resolver | Phytron RO2010-386 | |
| Switch | Marquardt 1010.3001 | |
| T-Sensor | PT-100 in motor | |

Note:
(1) The coordinate system of NIX is oriented such that X is parallel to the optical (or rotational) direction of the mechanisms, and Z is parallel to the main axis of the telescope (vertical direction for the mechanisms relative to the bench).

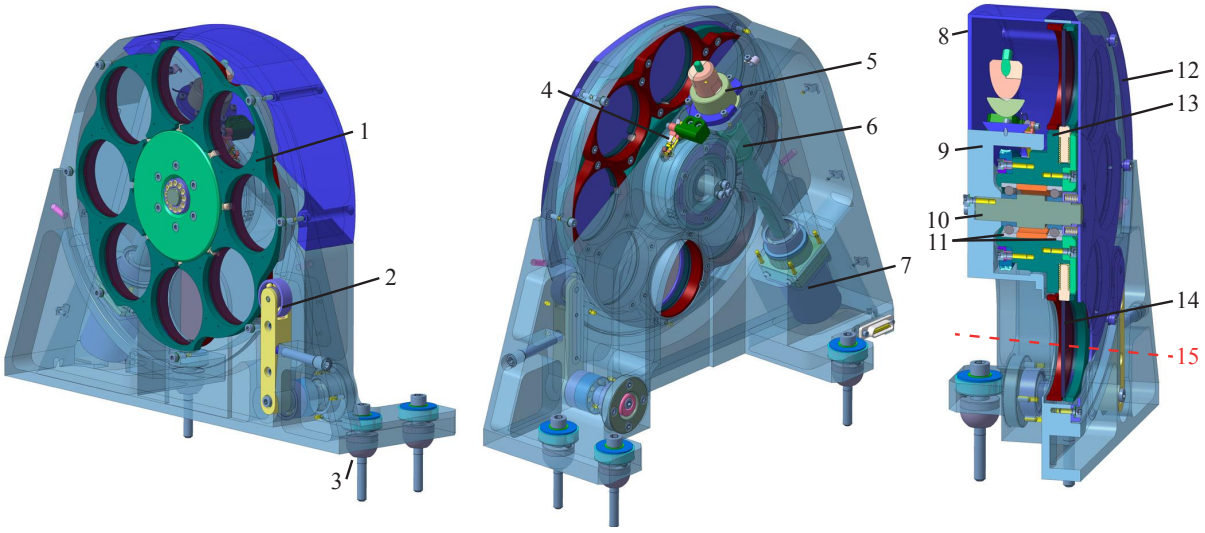


Figure 2. Design overview of the APW with transparent housing: The left panel shows the APW seen from the NIX entrance window with the aperture wheel (1), the pre-load lever (2), and the mounting interface to the NIX optical bench (3). The mid panel shows the opposite side seen from the detector side with the home switch (4), resolver (5), worm gear (6), and the stepper motor (7). The right panel shows the cut-view parallel to the optical and rotation axes with the housing top cover (8), main structure (9), central shaft (10), bearings (11), housing front cover (12), gear wheel (13), aperture elements (14), and the optical axis (15).

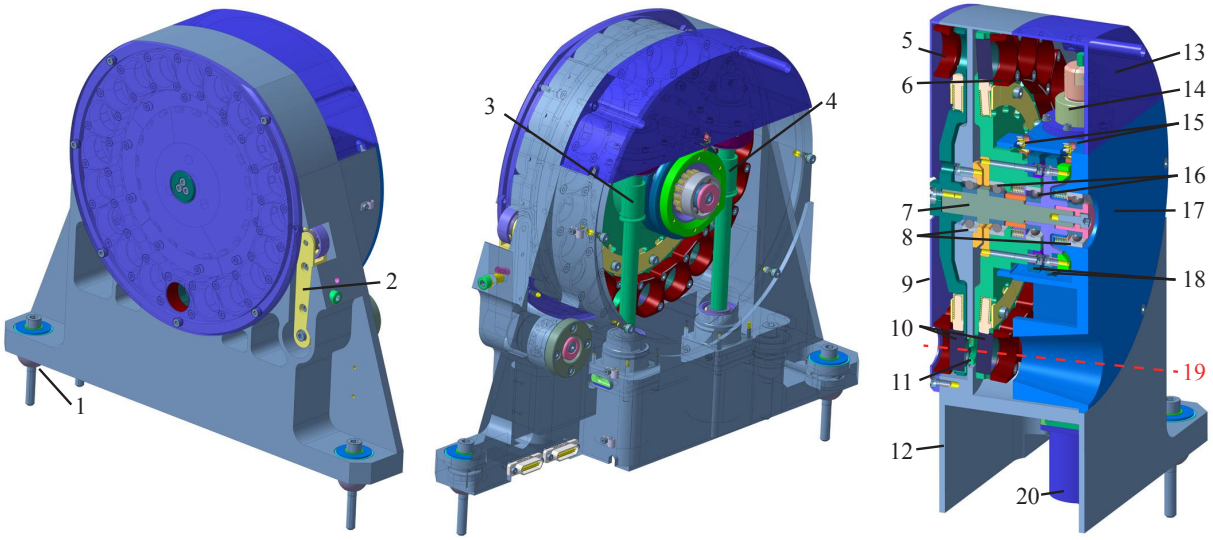


Figure 3. Design overview of the PFW with semi-transparent housing: The left panel shows the PFW seen from the detector side with the mounting interface to the NIX optical bench (1) and the pre-load lever (2). The mid panel shows the opposite side seen from the entrance of NIX with the worm gears for the filter (3) and pupil wheel (4). The right panel shows the cut-view parallel to the optical and rotation axes with the pupil wheel (5), filter wheel (6), central shaft (7), bearings for the pupil wheel (8), housing front cover (9), pupil masks and filters (10), Fixed Cold Stop (11), main structure (12), housing top cover (13), resolver for pupil wheel (14), home switches for both wheels (15), bearings for the filter wheel (16), housing front structure (17), gear wheels (18), the optical axis (19), and the stepper motor for the pupil wheel (20).

motor when the wheels are not rotated. To improve the position stability and accuracy, the aperture wheel and the pupil wheel are pre-loaded by a spring-loaded lever that pushes the wheel in tangential direction when the wheel slots are at the nominal position. With this pre-loading, the position accuracy becomes independent of the gear play. The filter wheel has no pre-loading, as first, the tolerances are much more relaxed and second, because no space was available to implement such a lever system.

For motion and position control, the motor axis is coupled to a resolver from Phytron of type RO2010. The resolver is used as a relative position reference to operate the mechanisms in closed-loop. For absolute position reference, a switch is triggered when a hunch mounted on the wheel is rotated to its nominal location.

### 3.2 Mechanical Design Description

Most parts of the PFW and APW are machined from aluminium alloy 6082. By using uniformly the same material, problems of differential thermal expansion can be prevented. However, a few parts have to made from different materials, in particular the gear wheel, which is made from PEEK (Polyether ether ketone) to serve as a dry lubricant. To overcome the different coefficient of thermal expansion (CTE) between the worm and the gear wheel, the gear play is adjusted such that it is optimised for the nominal temperature at 75 K while at ambient temperatures, the play increases. The gear play is fine-tuned during the test campaign as the separation of the motor axis is adjustable relative to the wheel. The bearings for the motor axes contain a PEEK cage. The different CTE to the aluminium housing and wheel shafts is taken into account by the correct mechanical tolerances at ambient temperatures. This means that the required tolerances will only be guaranteed at cryogenic condition while at ambient temperatures, the functions are still provided but with less accuracy.

The APW housing is monolithic and provides the stationary mounted main central shaft. The rotatable wheel assembly is mounted to the central shaft using two bearings made from stainless steel with ceramic balls.

The housing of the PWA consists of two main parts, the main structure and the front structure. The main structure provides the stiff interface between the attachment feet, the Fixed Cold Stop (FCS) and the rotation

axis. The front structure is used to hold the motor assemblies and to apply the axial force for the clamping of the wheel's bearings. The central shaft is mounted with two bearings to the housing and fixed with the pupil wheel assembly. The filter wheel assembly is mounted to the central shaft with another pair of bearings. This implies that for a rotation of the pupil wheel, all four bearings are in motion (assuming that the filter wheel is not turned simultaneously). To ensure maximum position accuracy of the pupil wheel elements, from each pair of bearings the one closest to the FCS is fixed while the other is axially spring loaded.

Two covers are used to fully enclose both mechanisms. These covers do not provide any additional functions.

### 3.3 Mounting concept for optical elements

We illustrate the mounting concept for the optical elements through the example of the pupil wheel. The principle for the other wheels is similar but simpler and varies only by the geometry.

The pupil wheel of the PFW provides space for 20 pupil masks that can be combined with filters. Figure 4 illustrates the concept of the packaging and mounting of these elements. In some observing modes, the combination of a band-pass filter (placed in the filter wheel) and either a neutral-density filter, a blocking filter or a glass dummy is required (see Section 2.1). To allow filters to be interchanged between both wheels of the PFW, the slot sizes are designed such that filters can be either placed in the filter wheel directly, or inside the pupil masks as shown in Figure 4.

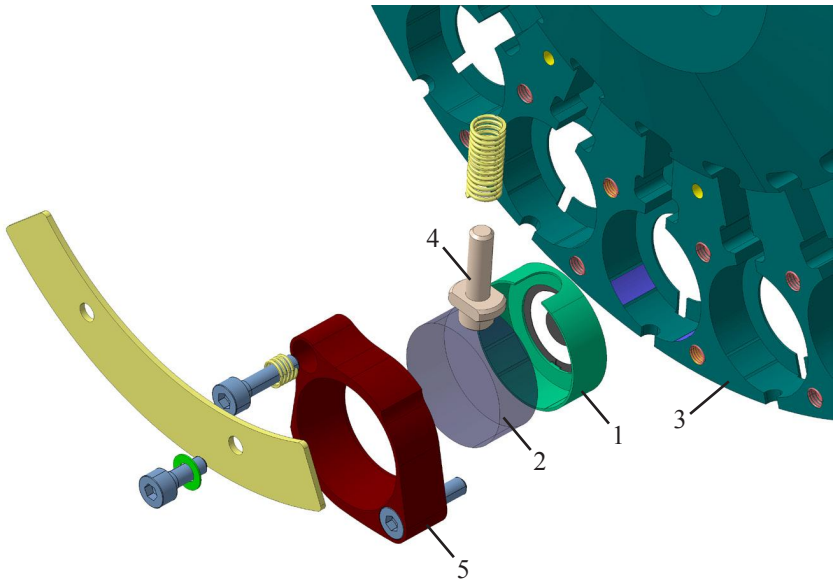


Figure 4. Exploded view of a pupil mask (1) combined with a filter element (2) mounted in the pupil wheel (3). A spring-loaded pin (4) and a filter/mask holder (5) provide the kinematic fixation of the elements.

The masks and/or filters are pushed radially by a spring loaded pin towards to well defined surfaces in the wheel (indicated in blue in Figure 4). This provides maximum accuracy for the lateral displacement of the pupil masks. To hold the elements axially in place, a spring loaded holder part pushes the element towards the end stop in the wheels. A notch in the wheel combined with a nose in the mask element determines the rotational position and locks it.

## 4. PERFORMANCE MEASUREMENTS

### 4.1 Overview and test setup

The APW and PFW underwent an extended test campaign for verification of the functions and quantification of the performances of the mechanisms. An extra effort has been taken to measure the achievable position accuracies

at cryogenic conditions. For this purpose, a dedicated cryo-test facility was developed[6] to accommodate the special needs for such a measurement. The goal was to measure optically the lateral displacement and tip/tilt accuracies while the mechanism is under nominal condition.

To measure the lateral displacement, we aimed for a measurement accuracy at micron level. Consequently, we needed an optical resolution in the sub-micron range. We concluded that this can be achieved by a good commercial macro lens (Canon EF100/2.8L) and camera, as it provides a better compromise between working distance and resolution when compared to microscopes. A measurement accuracy of 0.2 $\mu$m has been confirmed in a pre-test. To achieve this resolution, we had to work at the minimum working distance of the lens (146 mm). Therefore, we had to build a setup with a very small distance between the optical window and the test specimen, also including radiation shields in between. Figure 5 shows the test facility that was built to address this dedicated need. The optical window is placed inside the circumference of the vacuum vessel and the thermal shields have been shaped as boxes not to increase the separation between a cylindrical shape and the test-specimen.

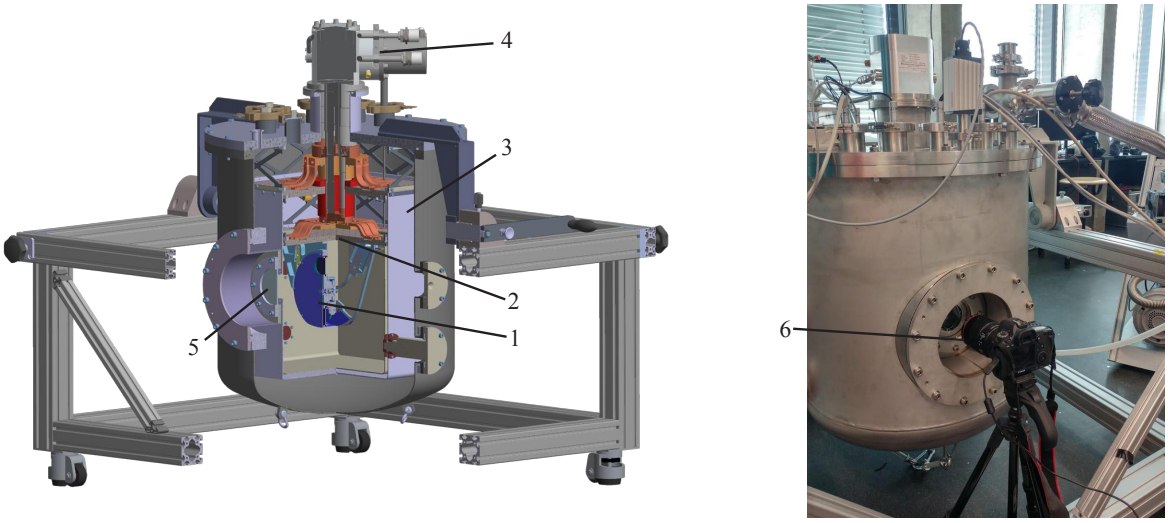


Figure 5. Setup for cryogenic characterisation tests of the APW and PFW: A cut-view of the test-cryostat (left) and an image of the measurement setup (right) shows the APW (1) mounted on the cold plate (2) and surrounded by radiation shields (3). The facility is cooled by a Pulse Tube Cooler (4). A large optical window (5) allows the measurement of position accuracy with a commercial camera (6).

## 4.2 Position accuracy

To measure the lateral position accuracy at cryogenic conditions, dedicated alignment masks are installed. Figure 6 shows the APW with one of these elements, providing a cross-hair to indicate the centre of the wheel slot. The element is back-illuminated by LEDs that are mounted inside the cryostat. Once the chamber is closed, the cross-hair elements are imaged by the camera. To calibrate the camera pixel size with the physical unit of the displacement, one of the wheel slots holds a glass element with a lithographic ruler that has a unit separation of 50 $\mu$m. The center of the cross-hair is determined relative to the camera chip.

To investigate the actual measurement accuracy, a series of pictures were taken without moving the mechanism. The scattering of the location of the cross-hair center is shown in Figure 7. The residual of $\pm$2.0 $\mu$m RMS is a result from the camera mount that does not provide high stability when the camera is excited due to the opening of the shutter. However, this limitation is acceptable as it is sufficient to verify the 15 $\mu$m position repeatability (see Table 3).

The resulting repeatability at cryogenic condition is equal or below the achieved measurement accuracy. We measure a peak-to-peak variation of $\sim$6.5 $\mu$m which is by more than a factor of 2 below the budgeted allocation

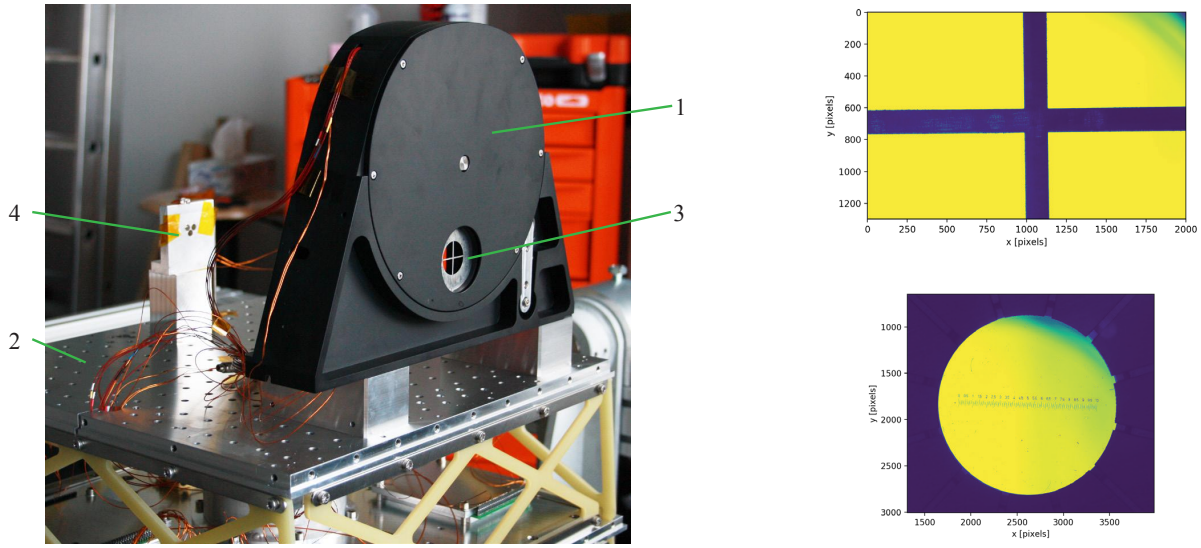


Figure 6. Left: APW (1) mounted on the cold bench (2) of the cryo-test facility. Cross-hair elements (3) for alignment tests are installed in the slots. A LED (4) provides the back-illumination of the elements. Top Right: Image of back-illuminated cross-hair element. Bottom Right: Image of back-illuminated lithographic ruler.

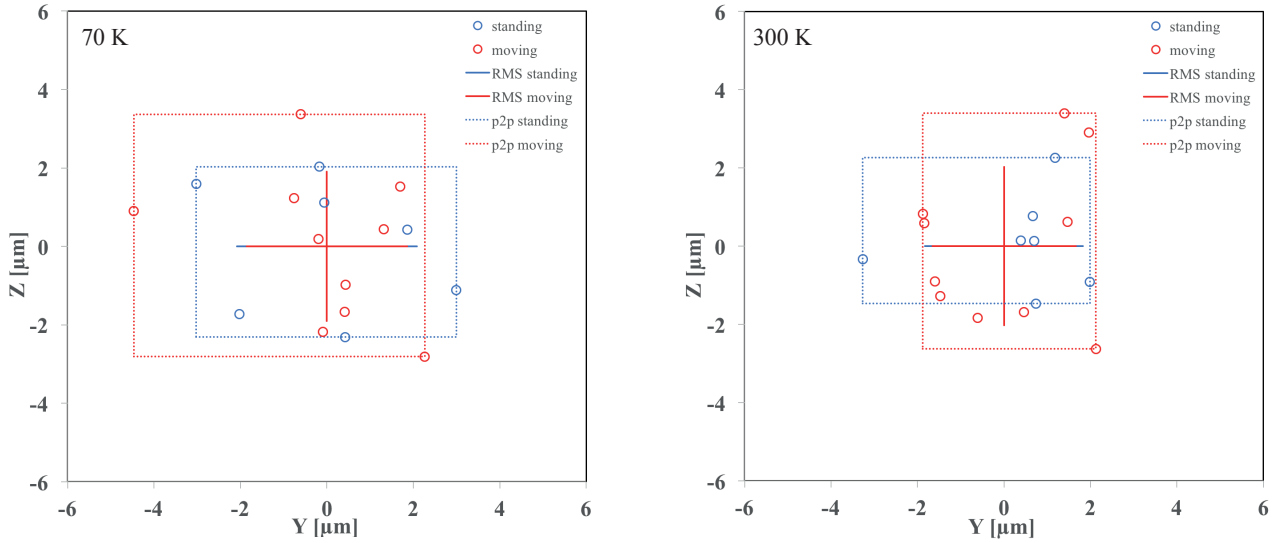


Figure 7. Result of the repeatability measurement for cryogenic (left) and ambient (right) conditions. The blue data show the measurement of the cross-hair center without moving the wheel, indicating the measurement accuracy limited by the setup. The red data show the measurement of the cross-hair center with repeatable movements of the mechanism. The maximum spread of data is indicated by the dashed rectangles while the crosses indicate the RMS.

for the repeatability. As this result is largely dominated by the measurement accuracy we can assume that the mechanism performs better. At ambient condition, the repeatability does not show any different characteristics.

## 5. SUMMARY

The performance tests of the APW and PFW show excellent performance and that the design is fully compliant with the required position accuracies. The concept of a pre-loaded worm-gear proofed to provide high reliable performance and accuracies. Early in the design phase the decision was made to provide the capability for

adjusting the gear game during the test campaign. This payed out very much as the optimum between induced friction and achievable precision can hardly be controlled just by manufacturing tolerances.

## ACKNOWLEDGMENTS

Parts of this work have been carried out within the framework of the National Center for Competence in Research PlanetS supported by the SNSF. AMG acknowledges the financial support of the SNSF.

## REFERENCES

[1] Davies, R. et al., "ERIS: Revitalising an Adaptive Optics Instrument for the VLT," *Proc. SPIE* **10702** (2018).

[2] Riccardi, A. et al., "The ERIS Adaptive Optics System: from design to hardware," *Proc. SPIE* **10703** (2018).

[3] Dolci, M. et al., "Final Design and Construction of the ERIS Calibration Unit," *Proc. SPIE* **10702** (2018).

[4] George, E. M., Gräff, D., Feuchtgruber, H., et al., "Making SPIFFI SPIFFIER: upgrade of the SPIFFI instrument for use in ERIS and performance analysis from re-commissioning," *Proc. SPIE* **9908**, 99080G (2016).

[5] Pearson, D., Taylor, W., Davies, R., et al., "NIX, the imager for ERIS: the AO instrument for the VLT," *Proc. SPIE* **9908**, 99083F (2016).

[6] March, S., Glauser, A. M., Baer, M., and Patapis, P., "A multi-purpose cryogenic test facility for astronomical instrumentation," *Proc. SPIE* **10706** (2018).